INT. J. REMOTE SENSING, 10 AUGUST, 2004,
VOL. 25, NO. 15, 3073–3090

Taylor & Francis
Taylor & Francis Group

On the LAI of mixed soils–forests regions

M. RAFFY*

Laboratoire de Sciences de l'Image, l'Informatique et la Télédétection (LSIIT), Parc d'Innovation, 5 Boulevard S. Brant, 67400 Strasbourg-Illkirch, France; e-mail: raffy@sepia.u-strasbg.fr

and K. SOUDANI

Laboratoire d'Ecologie Systémique et Evolution, Département Ecophysiologie Végétale Université Paris-Sud XI, Bat. 362, 91405 Orsay Cedex, France; e-mail: kamel.soudani@ese.u-psud.fr

(*Received 25 February 2002; in final form 10 August 2003*)

Abstract. In homogeneous forest textures, it has been recently confirmed experimentally that, for sufficiently large ground surfaces, the Leaf Area Index (LAI) has weak variations with respect to ground surface variations. This allows computing the LAI of mixed pixels on regions composed of forests and soils, with the use of the Perpendicular Vegetation Index (PVI). In the present paper, we study the accuracy of the method with experimental data.

1. Introduction

One of the permanent difficulties in the use of Earth remotely sensed data is to take into account the heterogeneity of the surfaces. On the other hand, in the study of the biomass, the Leaf Area Index (LAI), is a key parameter. The LAI in consideration here is the vertical projection of the total foliage surface per unit of soil surface. For example, the LAI considered as a parameter depending on the vertical distance to the soil, at a given altitude (Hapke 1993), is not a useful definition for our topic.

In the light of recent experimental results on the spatial variability of forest LAI (Raffy *et al*. 2003), we study a simple formula proposed by these authors, giving the LAI of mixed pixels. In the following, so that it will not be ambiguous, we call pixel or ground-pixel the ground area (the instantaneous field of view) corresponding to an image pixel (figure 1).

We consider forests where the distribution of foliage aggregates has a regular statistical aspect at a large scale. Many forests have such a distribution, when they are composed of one or a few species naturally spaced. Figure 1(*a*) shows such a forest, observed from an airborne, in the Système Probatoire de l'Observation de la Terre (SPOT) XS channel 2, at the resolution of 2 m.

*Corresponding author.

International Journal of Remote Sensing
ISSN 0143-1161 print/ISSN 1366-5901 online © 2004 Taylor & Francis Ltd
http://www.tandf.co.uk/journals
DOI: 10.1080/01431160310001632693

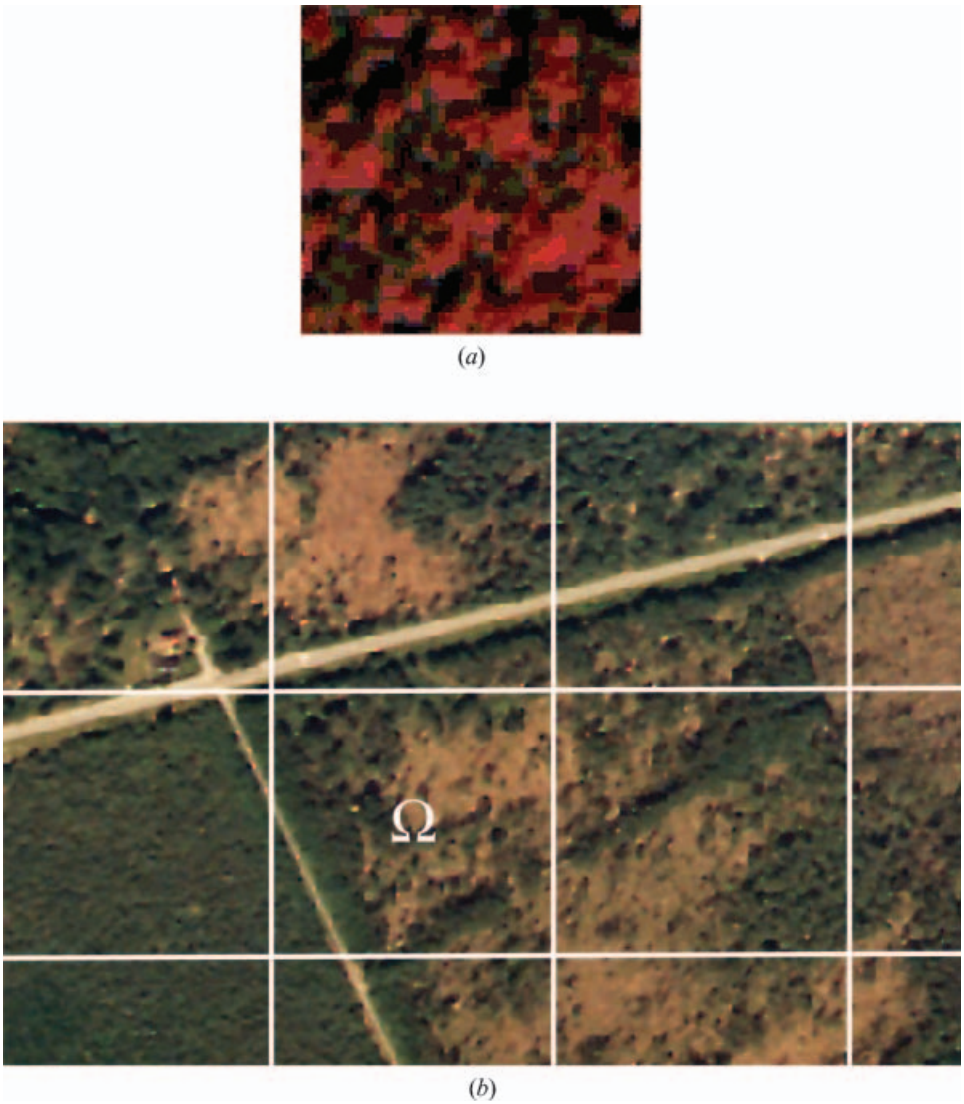

Figure 1. (*a*) Radiometric view (channel XS2) of the homogeneous forest plot A, at a resolution of 2 m. (*b*) Type of landscape considered in the study. The size of Ω is not at the scale of the SPOT XS pixels (20 m × 20 m).

Two results had been pointed out by Raffy *et al*. (2003). First, they measure how, when the extension of the area of the vertical projection Ω of the forest on the soil increases, the LAI variation decreases and the LAI value tends to a constant value λ. For example, they show that the difference between the asymptotic value λ and the actual one measured on Ω, is less than 20% when the size of the surface Ω overpasses the size of a 30 m × 30 m square, for the forest of figure 1(*a*). The notion of homogeneous forest is presented in a probabilistic way in the above-mentioned paper, but is not easy to characterize in practice, as is the case in many domains of natural sciences. We refer to this paper for a detailed discussion of this point and we consider here that a terrain experiment, a local high-resolution image

analysis or any *a priori* knowledge can allow to consider the forest as being homogeneous.

The second result states that for a ground-pixel Ω composed of a textured forest and various soils (figure 1), if we note

$$\vec{L}(\Omega) = \left(L^{(\mathrm{vis})}(\Omega),\, L^{(\mathrm{nir})}(\Omega)\right)$$

the measured radiance of Ω, in a visible channel (vis) and a near-infrared channel (nir), the LAI of Ω is given by

$$\mathrm{LAI}(\Omega) \approx \lambda \frac{\mathrm{PVI}\left(\vec{L}(\Omega)\right)}{\mathrm{PVI}\left(\vec{L}_V\right)} \tag{1}$$

In formula (1), PVI is the Perpendicular Vegetation Index defined by Richardson and Wiegand (1977) as the distance of $\vec{L}(\Omega)$ to the soils line. The denominator of (1) is the distance of the centre $\vec{L}_V$ of the radiometric domain of the forest to the soils line. Let us recall that the distance of $\vec{L}(\Omega)$ to the soils line is given by

$$\mathrm{PVI}\left(\vec{L}(\Omega)\right) = \frac{\left|L^{(\mathrm{nir})}(\Omega) - \left(aL^{(\mathrm{vis})}(\Omega) + b\right)\right|}{\sqrt{a^2+1}}$$

where a and b are defined by the soils line equation $L^{(\mathrm{nir})}(\Omega) = aL^{(\mathrm{vis})}(\Omega) + b$ exactly.

Remark 1.1: Let us suppose that the soils radiance describes a line and that the forest radiance is reduced to one given point $\vec{L}_V$ of the (vis–nir) radiometric domain. In this case, we have exactly

$$\frac{\mathrm{PVI}\left(\vec{L}(\Omega)\right)}{\mathrm{PVI}\left(\vec{L}_V\right)} = w$$

where w is the percentage of forest cover within Ω (see for example Raffy *et al.* 2003). Then, with these hypotheses, the relation (1) is no more than $\mathrm{LAI}(\Omega) = \lambda.w$.

Remark 1.2: Any relation giving the LAI from the radiometry is *a priori* suspicious. Indeed, a given distribution of trees on the surface (see, for example, figure 1(*b*)) has a fixed LAI, while the radiometry of the surface changes during a day. This point will be discussed in the next section, to make explicit the sense of (1).

In the present paper, we propose to estimate the validity of the formula (1) at the light of radiometric airborne and SPOT satellite data of forests and bare soils where the terrain LAI measurements had been experimentally obtained. In §2, we describe the previous data. In that section, we give the simulation procedure for the mixed pixels. In §3, we compute the LAI with (1) on mixed pixels, with systematic variations of the mixture components, which are soils and forest. The error is studied. Namely, we study the difference between the computed LAI from (1) as it may appear in the operational use of the formula and the LAI of the simulated pixels. We take into account all the factors which may generate a gap between the computed value (1) from satellite data and the actual value.

2. The measured and simulated data

2.1. *Radiometric and LAI measurements*

Three forest plots were chosen for this study. These plots, called A, B and C, are formed by $100\,\mathrm{m} \times 100\,\mathrm{m}$ squares. In the French National Forests Office (ONF)

their exact references are N° ONF 215, 003 and 1054. They are situated in the Alsacian plain (France), 48°5′ latitude, 7°55′ longitude, with a mean altitude of 130 m. The forest present on plot A is basically formed by oak (*Quercus robur* L.), beech (*Fagus sylvatica* L.) and hornbeam (*Carpinus betulus* L.) Plot B is composed of an almost pure beech grove. On plot C, the forest is an oak grove with beech undergrowth. The topography of the plot is flat.

2.1.1. *LAI measurements*

The LAI was measured after the fall of leaves (beginning of November 1997). The forest plots B and C were divided into 100 squares $10\,m \times 10\,m$, and A into 400 squares $5\,m \times 5\,m$. In each elementary square, the LAI was measured by 20 samples, following the 'point quadrat' method (Warren Wilson 1959, 1960, 1963) applied to the leaf fall after the complete fall of leaves (Nizinsky and Saugier 1988, Sabatier 1989, Dufrêne and Bréda 1995). This method consists in vertically introducing a thin needle of approximately 2 mm in diameter into the leaf fall and counting the pierced leaves stuck on the needle. The operation is repeated 2000 times (plots B and C) and 8000 times (plot A) to obtain an estimation of the leaf fall. The sampling error is summarized in the confidence interval, which is the interval where belongs the asymptotic value λ with a given probability.

The mean LAI on the total plots A, B and C are

$$\lambda_A = 6.15 \quad \lambda_B = 5.05 \quad \lambda_C = 5.34 \tag{2}$$

and the exact mean, for ever unknown exactly is, with a probability of 95% within the intervals

$$I_A = [6.02, 6.28], \quad I_B = [4.91, 5.18], \quad I_C = [5.12, 5.57] \tag{3}$$

2.1.2. *Radiometric measurements (ARAT aircraft and SPOT satellite)*

During the following summer season (July 1998), these plots of forest were flown over, around 11.00 am, by an aircraft (the Avion de Recherche Atmosphérique et de Télédétection (ARAT) of the CNRS). It registered the area radiance in the wavebands [610 nm, 680 nm] and [790 nm, 890 nm], corresponding to channels 2 and 3 of SPOT XS, with a resolution of 2 m (figure 1(*a*) and (*b*)). Simultaneously, the radiance of bare soils and shadowed soils were measured, in the same area, in the same geometrical conditions by this aircraft. A SPOT XS image of the region (at 20 m resolution), taken on the same day (21 July) and at the same time (11.00 am), is also used.

Finally, the measurements are constituted with:

(a) three plots of forest A, B, C, with given textures on which the values λ_A, λ_B, λ_C of the LAI are known with a definite precision (below noted λ, in a generic manner);
(b) radiometric values in the visible and near-infrared bands (same as XS2 and XS3 channels of SPOT), at the resolution of 2 m on the forest plots (figure 1(*a*)) and its surroundings (figure 1(*b*)). They concern:

(b1) the plots of forest, and
(b2) bare soils clear and shadowed; and

(c) at 20 m resolution, SPOT XS data of the region, channels XS2 and XS3 (channels 2 and 3 of the XS radiometer).

2.2. *Simulation of mixed pixels*

In order to have an exhaustive set of pixels with all the percentages of forest and soils, we composed the pixels with the radiometric data (b1) and (b2). We composed 100 squares 20 m × 20 m with various ratios of components. Each square was obtained by drawing at random the origin of a 20 m × 20 m square within the forest high-resolution data. The same operation was realized in the bare soils high-resolution area. Then, following the operation described in figure 2, a part of each square was picked up in a ratio of w in the vegetation square and 100 minus w in the bare soils one, to compose one 20 m × 20 m pixel. Two such pixels are presented in figure 2.

Finally, we have a set of 100 mixed squares 20 m × 20 m. This set is ordered by the increasing forest cover percentage w, from $w = 1\%$ to $w = 100\%$, with a step of 1%. This operation can be repeated many times for each value of w.

The LAI of each pixel Ω is equal to $\lambda.w$, where λ is the estimated experimental LAI of the forest plots. Following the choice of forest plot A B or C, λ is given by the centre of the confidence intervals (3). We shall note $\mathrm{LAI}^{ex}(\Omega) = \lambda.w$ this reference LAI, which is the exact physical value (with a probability of 95%) of the leaves' surface reported to the surface of Ω.

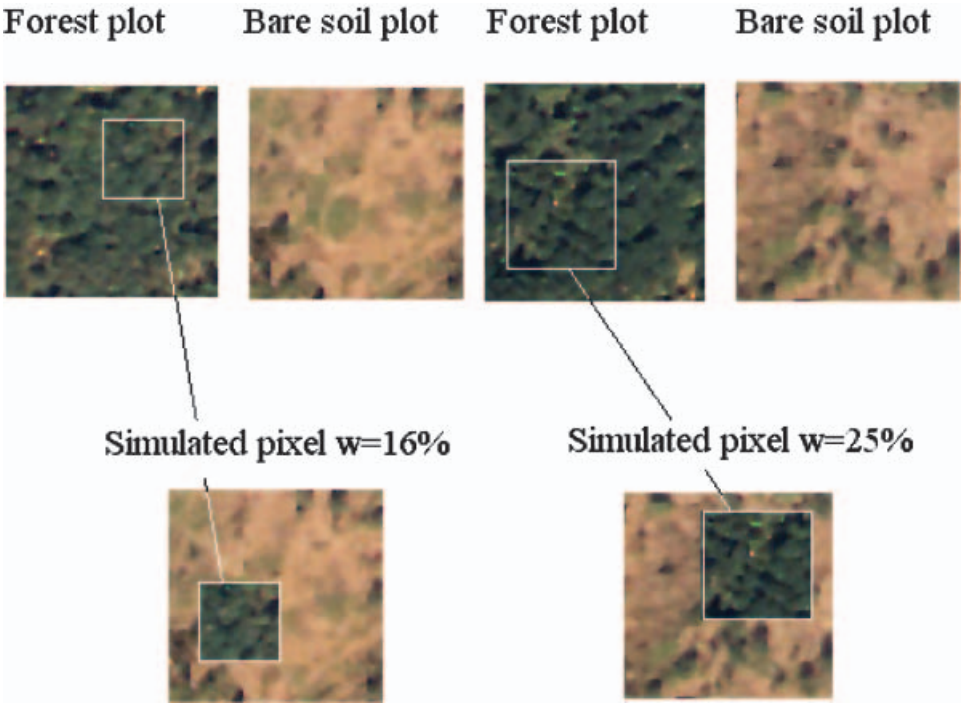

Figure 2. Pixels simulation. Forest and bare soil square areas are randomly defined. Then, in the forest area, a ratio w% is picked up and substituted in a same square area of the bare soil. Two such operations are represented with $w = 16\%$ and 25%. If the shadow effect is considered (§ 4.2), a ratio shad(w)% is substituted in a same area of the bare soil, exactly as the forest part.

Then, for each simulation of Ω, the airborne radiometric measurements of the $20\,\mathrm{m} \times 20\,\mathrm{m}$ pixels is computed as the average values of the high resolution ones. We thus obtain a value $\vec{L}(\Omega) = \left(L^{\mathrm{vis}}(\Omega), L^{\mathrm{nir}}(\Omega)\right)$, for each simulated pixel Ω.

Remark 2.1: This last computation relies on the hypothesis that the low-resolution radiance is measured with a perfect sensor. In fact, even this point does not specifically concern the study of the quality of the formula (1), it must be taken in mind, since we are led to compare *in situ* values of the LAI with the computed value using radiance filtered by the non-perfect radiometer.

Remark 2.2: The continuity of the forest or bare soils area picked up to constitute the simulated pixels is necessary to maintain the natural texture (i.e. the statistical properties of the radiance distribution) of the scene.

3. First testing of formula (1)

For each forest percentage w within Ω, we are now able to compute the LAI of Ω using (1). Indeed, for each choice of forest type, A, B or C, the radiometric domain is known (data (b1), §2.1), then we obtain $\vec{L}_V$ in each case. We know also the soils line (data (b2)). The computed value of the LAI will be noted $\mathrm{LAI}^{\mathrm{comp}}(\Omega)$. It is compared to $\mathrm{LAI}^{\mathrm{ex}}(\Omega)$ (figure 3) for all the forest percentages w, from 1% to 100%, for each type of forest A, B and C. The slight fluctuations around the straight line come from the fact that for each outcome of Ω, the radiometric domain of Ω is no more reduced to the soils line and the point $\vec{L}_V$. Table 1(*a*) indicates the mean and standard deviation around the straight line of figure 3.

Despite these slight fluctuations, figure 3 confirms the validity of formula (1), at least from a theoretical point of view. While for each outcome Ω, $\mathrm{LAI}^{\mathrm{ex}}(\Omega)$ is fixed, the radiometry of Ω, as it can be measured by the satellite, may be different from $\vec{L}(\Omega) = \left(L^{\mathrm{vis}}(\Omega), L^{\mathrm{nir}}(\Omega)\right)$, computed behind with the high-resolution data. Then the value

$$\lambda \frac{\mathrm{PVI}\left(\vec{L}(\Omega)\right)}{\mathrm{PVI}\left(\vec{L}_V\right)} \tag{4}$$

computed with satellite data may create such a gap that (1) becomes of no interest in operational applications. In the next section we consider all the possible perturbations on (4), in the operational use of formula (1).

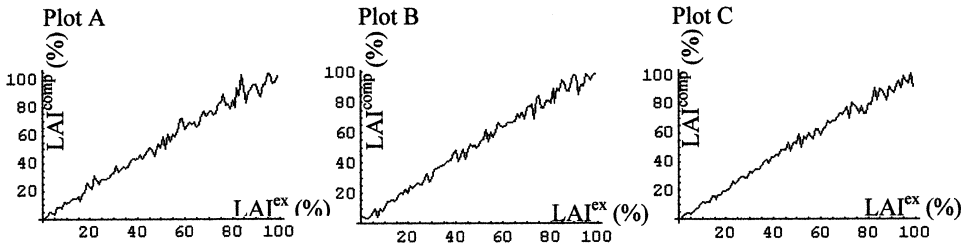

Figure 3. Computed values of $\mathrm{PVI}\left(\vec{L}(\Omega)\right)/\mathrm{PVI}\left(\vec{L}_V\right)$ for simulated SPOT pixels using forest plots A, B and C, for $w = 1-100\%$. The fluctuations around the straight line are due to the radiometric heterogeneity of the forests and bare soils.

Table 1. Quality of the approximation presented in figure 5.
(*a*)

Simulation using forest plots A, B and C without shadow	A (%)	B (%)	C (%)
Mean error	2.56	2.42	2.01
Standard deviation	2.75	1.95	1.72

(*b*)

Simulation using forest plots A, B and C with shadow	A (%)	B (%)	C (%)
Mean error	3.58	3.52	2.23
Standard deviation	2.96	2.52	1.65

4. Perturbations of the radiometry and operational use of formula (1)

For a given distribution of trees on the ground surface, the LAI is fixed. Nevertheless, following the hour of the day, the radiometry is not the same. This obvious phenomenon could lead to rejection of any relationship giving the LAI from the radiometry. In fact, (1) and all these types of formula cannot be exact because, while the physical LAI has a given value, various parameters modify the measured radiometry and change the numerical value of (4). These parameters are mainly:

– the radiometric heterogeneity of the forest and the soils pointed out in figure 3 and Table 1(*a*);
– the trees' shadows on the bare soil;
– the atmospheric effects; and
– the angular effects of the Sun and of the sensor.

In this section, we shall study the role of the previous parameters on $\vec{L}(\Omega)$ and $\mathrm{LAI}^{\mathrm{comp}}(\Omega)$.

4.1. *Radiometric heterogeneity of forest and soils components of* Ω

This effect is present in the simulated pixels and reported in figure 3 and Table 1(*a*). Without radiometric heterogeneity of the forest and soil components of Ω, we should observe an exact straight line.

Let us remark that the foliage clumps have a variable shadow effect on the radiometry, following the Sun incidence. This effect, studied in Leblanc *et al.* 2001, is, in our study, measured at the instant of the airborne measurements. The various perturbations on (4) mentioned at the beginning of §4 are studied at the instant given by the data (here, at 11.00 am).

4.2. *Shadow effect*

The previous simulations (figure 2) take into account only the shadow of the bare soils and of the dense forest, but not any effect of the shadow due to the trees' dispersion on the ground. We may improve the radiometric simulation by introducing a shadow effect due to the sparseness of the forest.

In the absence of vegetation ($w=0$), on a flat soil Ω, the shadow effect of the

vegetation on the radiometry is null. This effect is again null when at the opposite, $w = 100\%$. Indeed, we have to consider only the shadow of the forest on the soil, since the shadow of the leaves' aggregates is included in the forest radiometry (forest plot, figure 2). Between these extreme values of w, the ground surface area covered by the shadow of the trees must increase from zero before decreasing to zero when w approaches 100%. If we note shad(w) the continuous function of w which measures the percentage of the ground covered by the trees' shadow within Ω, we remark that we must strictly have $w + \text{shad}(w) \leqslant 100\%$. Furthermore, the case where $\text{shad}(w) = w$ seems to be a very high shadow percentage within Ω, at the moment of the data acquisition. Then, we may consider that $\text{shad}(w) \leqslant w$.

Finally, in order to respect these various conditions, we propose the function

$$\text{shad}(w) = (100 - w)\sqrt{w/100}$$

in % (figure 4) to express the shadow due to the vegetation sparseness at a given time of the day. This choice has the advantage of simplicity.

Remark 4.1: We cannot simulate a too sparse trees distribution without modifying the value λ obtained in a compact forest. The shape of the shadow function (figure 4) takes this remark qualitatively into account.

In the constitution of the mixed pixels, §2.2, we had $\text{shad}(w) = 0$ for any value of w. To take into account the shape and sparseness of the forest following the function shad(w), we used pure shadowed area viewed by the aircraft and we selected randomly a square of surface area $|\Omega|.\text{shad}(w)/100$ added within Ω, in place of the same area of bare soil.

The computation leading to figure 3 was done again with the shadow effect on the simulated pixels, for increasing values of w. Table 1(b) compared to Table 1(a) shows that the shadow of trees provokes a slight increasing of the error on the LAI computed by (1).

Figure 5 presents the effect of the shadow function on the radiometric domain

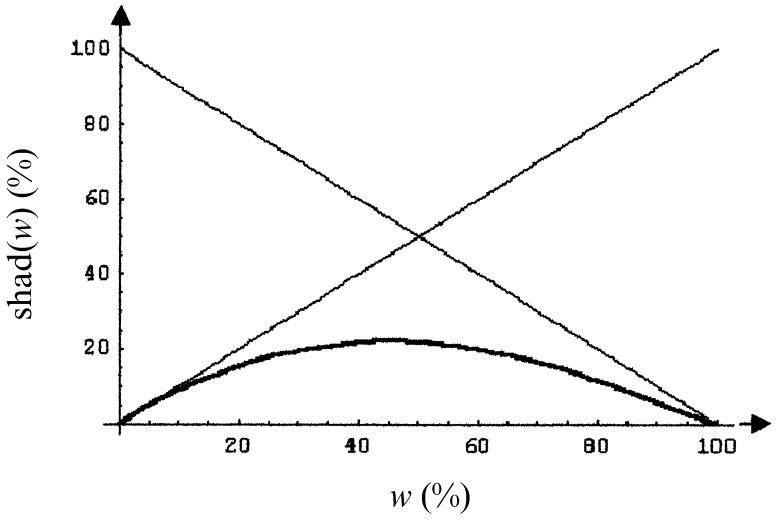

Figure 4. The bold curve $\text{shad}(w) = (100 - w)\sqrt{(w/100)}$ in %, satisfies the conditions $w + \text{shad}(w) \leqslant 100\%$ and $\text{shad}(w) \leqslant w$. The limits of these two conditions are represented by the two straight lines. For a w percentage of forest within Ω, shad(w)% of shadowed soil is substituted in a same area of the bare soil part of Ω.

(in the channels XS1 and XS2 of SPOT) for 35 simulated pixels Ω. We compare the radiometry of the mixed $20\,\mathrm{m} \times 20\,\mathrm{m}$ pixels Ω without shadow effect (figure 5(*a*), (*b*) and (*c*)) with the same pixels with shadow effect (figure 5(*d*), (*e*) and (*f*)). In this figure, we first recognize the classical positions of the bare soils and of the vegetation (forest plots A, B and C). The radiometric values of the 35 simulated pixels correspond to the clusters of points in the centre of these domains. The perturbation of the shadow effect on the radiometry is not negligible, while it is weak on (4) (see table 1).

On these radiometric domains, we superimposed (bold points) the SPOT data of the same region. The exact geographical superimposition of the airborne and the 25 SPOT pixels is not possible. Then, figure 5 is just qualitatively significant. Nevertheless, we observe a best superimposition of the SPOT data on the simulated pixels without shadow in the cases of figure 5(*a*) and (*b*). This can be due to the impossibility of an exact superimposition as well as to angular and atmospheric effects on SPOT data.

Since the shadow effect enhances the radiometric realism of the pixels simulation, this effect will systematically be included in the following.

4.3. *Atmospheric and angular effects*

The atmosphere, the sensor's properties and its angular position are parameters which also modify the radiometry of Ω, in a non-negligible manner. These parameters play in two different scales on the measured data.

At the local scale, the combination of atmosphere and the three-dimensional geometry of the various components of Ω provokes a 'radiometric contagion' of the elements. This local effect depends also on the angle of view. The consequence on the radiometry is an individual translation of $\vec{L}(\Omega)$ for each Ω.

In addition to the local effect, the atmosphere and the angular difference of the airborne and satellite measurements play at the large scale, on the whole image. In other words, these effects influence mainly the global geometry of the radiometric domain, while the local effects modify separately the positions of the points $\vec{L}$.

Then, in order to take into account the role of atmosphere and angle of view, we shall observe the behaviour of (4), with respect to translations on $\vec{L}$ in the radiometric domain. In fact, compared to the global ones, the local effects have the first-order influence on the numerical value of (4), because global translations on the radiometric domain do not modify the PVI.

5. Numerical influence of the previous effects on the computation of (4)

The various causes for the gap between the exact terrain $\mathrm{LAI}^{\mathrm{ex}}(\Omega)$ and $\mathrm{LAI}^{\mathrm{comp}}(\Omega)$ are listed above. We shall now numerically estimate the amplitude of these effects.

5.1. *Radiometric heterogeneity of the forest and the soils*

The role of this heterogeneity has been numerically estimated on (4), figure 3 and Table 1(*a*). These fluctuations on (4) correspond to the extension of the forest and bare soils radiometric regions of figure 5. The numerical effect of this heterogeneity on $\vec{L}(\Omega)$ can be estimated by the standard deviations $\mathrm{d}L^{(\mathrm{vis})}$ and $\mathrm{d}L^{(\mathrm{nir})}$ of the set of forest points and bare soils points in figure 5. We obtained with 100 simulated pixels, composed with $w = 50\%$: $\mathrm{d}L^{(\mathrm{vis})}/L^{(\mathrm{vis})} \approx 7\%$ and $\mathrm{d}L^{(\mathrm{nir})}/L^{(\mathrm{nir})} \approx 4\%$ (these values differ by less than 0.1% between the forest plots A, B

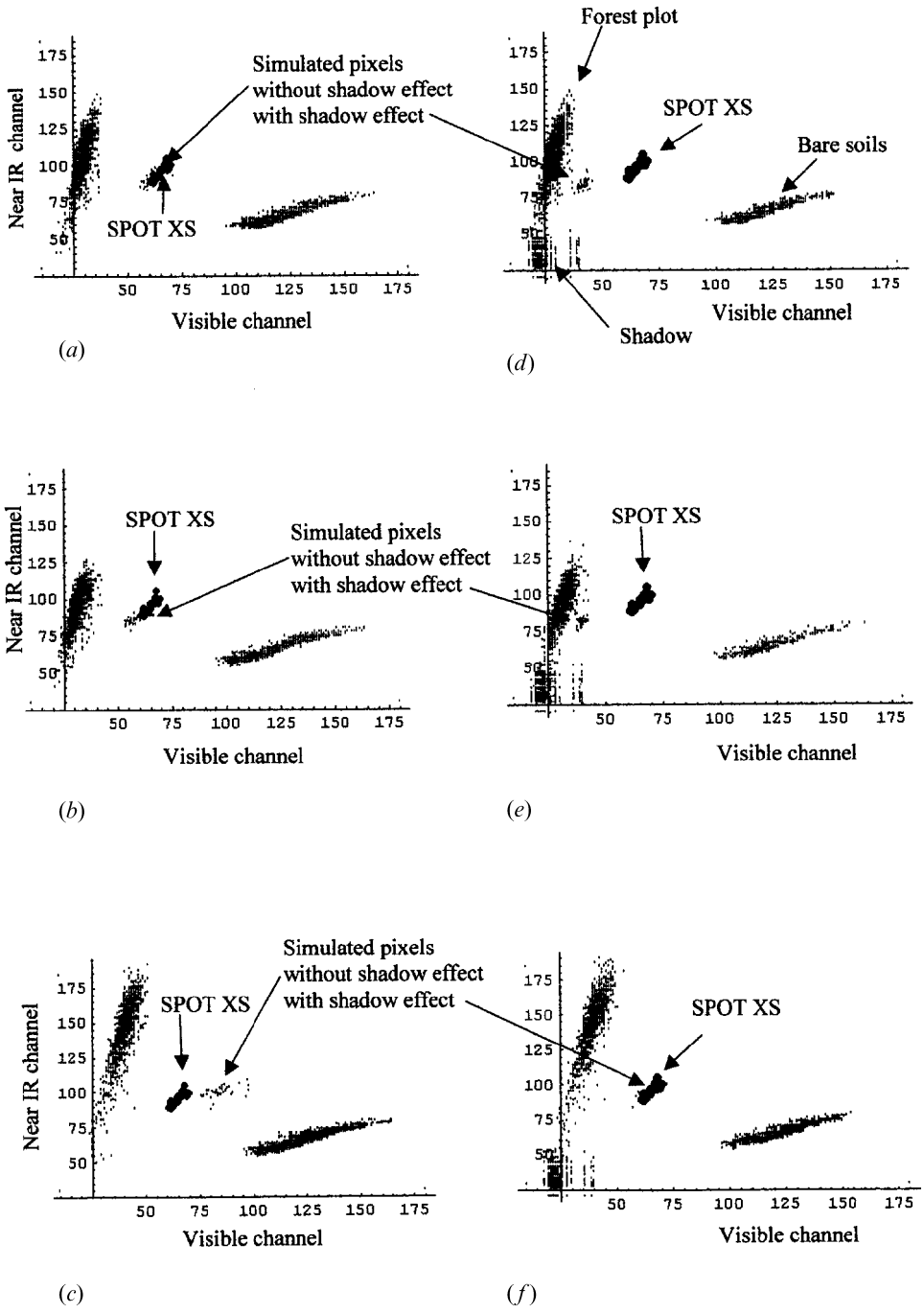

Figure 5. For each forest plot A, B and C, radiometric domains in the XS2 and XS3 channels of SPOT are represented. (*a*), (*b*) and (*c*) The left side domains represent the bare soils (at 2 m resolution) and the forest (at 2 m resolution). Superimposed are: the domains of the simulated 20 m × 20 m pixels (small dots); and the SPOT pixels of the same region (large dots). (*d*), (*e*) and (*f*) The right side is the same representation with the shadow effect. The shadowed soils are in the lower part of the graphs, the simulated pixels have their domains translated. We observe that the simulation of the SPOT pixels is better without shadow for forest plots A and B, while it is enhanced for forest plot C. (*a*), (*d*), Forest plot A. (*b*), (*e*), Forest plot B. (*c*), (*f*), Forest plot C.

and C). In fact, these values will not be directly useful in our study, because the clumping effect is already taken into account in the radiometric pixel simulaton.

In the same way, the radiometric effect of the shadow of the trees on the bare soils can be estimated by the mean displacement of the sets of points of mixed pixels when we go from the left to the right in figure 5. We obtained with 100 simulated pixels and $w = 50\%$: $dL^{(\mathrm{vis})}/L^{(\mathrm{vis})} \approx 27\%$ and $dL^{(\mathrm{nir})}/L^{(\mathrm{nir})} \approx 8.2\%$ for compositions with forest plot A, $dL^{(\mathrm{vis})}/L^{(\mathrm{vis})} \approx 28\%$ and $dL^{(\mathrm{nir})}/L^{(\mathrm{nir})} \approx 8.7\%$ with B and $dL^{(\mathrm{vis})}/L^{(\mathrm{vis})} \approx 25\%$ and $dL^{(\mathrm{nir})}/L^{(\mathrm{nir})} \approx 5.8\%$ with C. These values confirm that, in a relative scale, the numerical radiometric fluctuations due to the heterogeneity of the scene are larger than their consequences on the LAI, computed with the expression (4).

5.2. *Error on the theoretical asymptotic value* λ

This value of the totally covering forest is estimated by λ^{est} after terrain experiments. This error is due to the non-exhaustive density of the terrain LAI measurements. It is given by the confidence interval, which ensures that with a given probability, the value λ belongs to the interval. For each forest plot A, B and C, the values λ^{est} and their confidence intervals, for a probability of 95%, are given in (2) and (3). We deduce the bounds of the relative errors:

$$\frac{|d\lambda|}{\lambda} \leqslant 2.110^{-2} \text{ for plot A, } \frac{|d\lambda|}{\lambda} \leqslant 2.710^{-2} \text{ for plot B, } \frac{|d\lambda|}{\lambda} \leqslant 4.310^{-2} \text{ for plot C} \quad (5)$$

5.3. *Error on the soils line and on* $\vec{\mathrm{L}}_{\mathrm{V}}$

The computation of (4) implies the knowledge of the soils line (values a and b, in the expression of the PVI) and of $\vec{L}_V$. We supposed in the previous section that the high-resolution radiometry is known, then we calculated the soils line and $\vec{L}_V$ at the best (the large spot and the centred line, figure 6(*a*)). In practice, the parameters a, b and $\vec{L}_V$ must generally be approximated from low-resolution data and estimated with values a^{est}, b^{est} and $\vec{L}_V^{\mathrm{est}}$. The values a^{est}, b^{est} will be drawn at random following a Gaussian probability with standard deviations defined by the two lines around the soils line (figure 6(*a*)). The standard deviations are numerically taken equal to 20%:

$$\frac{|da|}{|a|} = 0.2 \text{ and } \frac{|db|}{|b|} = 0.2 \quad (6)$$

The values of $\vec{L}_V^{\mathrm{est}}$ are drawn at random in the same conditions with standard deviations of 10%:

$$\frac{\left|dL_V^{(\mathrm{vis})}\right|}{\left|L_V^{(\mathrm{vis})}\right|} = 0.1 \text{ and } \frac{\left|dL_V^{(\mathrm{nir})}\right|}{\left|L_V^{(\mathrm{nir})}\right|} = 0.1 \quad (7)$$

around the exact centre $\vec{L}_V$ used in the computations of §3. Figure 6 illustrates the random process (normal law): 100 outcomes of $\vec{L}_V^{\mathrm{est}}$ are represented by the 100 small points and by the same number of soils lines (figure 6(*b*)) defined by random values of a^{est} and b^{est}. In this figure, the contour line is the convex hull of the radiometric domain of the forest plot A.

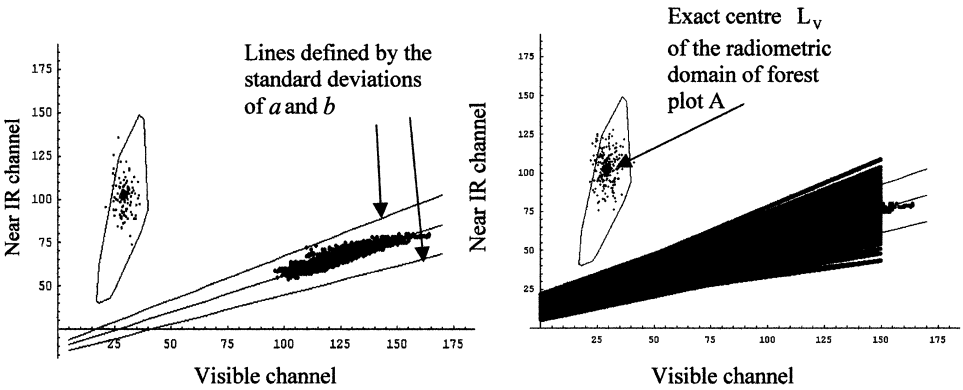

Figure 6. Error simulations on the input parameters. The large dot, within the radiometric representation of the forest, is the exact centre (the centre of gravity) of the domain, bounded by a contour line. The small dots are the points randomly picked up around the previous one and used for the computation of the LAI. (*a*) The thin straight lines are: the soil line, exactly obtained by the least-square method with the bare soils domain; and the lines defined by the standard deviations of a and b (equation (6)). (*b*) The random soils lines used for the computation of the LAI are superimposed.

5.4. *Atmospheric and angular effects*

The role of atmosphere and view angle on the radiometry is difficult to estimate numerically, although they appear in any use of satellite data (Kaufman 1989, Cracknell and Hayes 1993, Schowengerdt 1997). In §4.3, we observed that for the study of (4), we must essentially take into account the high-resolution effects of these parameters. For the simulations of errors which will follow, we estimated that these combined local effects can be integrated in the range of 10% taken in (7).

6. Numerical results

We have now all the elements to estimate the quality of the LAI computed by (1). Namely, we shall numerically study the two following values: $|\mathrm{LAI}^{\mathrm{ex}}(\Omega) - \mathrm{LAI}^{\mathrm{comp}}(\Omega)|$ and $|\mathrm{LAI}^{\mathrm{ex}}(\Omega) - \mathrm{LAI}^{\mathrm{comp}}(\Omega)|/\mathrm{LAI}^{\mathrm{ex}}(\Omega)$. We shall proceed in two complementary ways. In §6.1, we shall simulate random perturbations to the radiometry, following the ranges defined in §5 and observe their effects on (1). In §6.2, we shall study the quality of (1) in order to know the more sensitive parameters to estimate for the best operational use of (1).

6.1. *Statistical simulations*

The numerical results below are obtained with the following procedure:

- two hundred drawing lots of λ^{est}, a^{est}, b^{est}, $\left(L_V^{\mathrm{nir}}\right)^{\mathrm{est}}$, $\left(L_V^{\mathrm{vis}}\right)^{\mathrm{est}}$ are randomly defined from normal laws with standard deviations given by (5), (6) and (7) (see figure 6(*b*));
- for each forest plot A, B and C: 15 simulated pixels Ω_i, with a prescribed value w of cover percentage; and

– computation of

$$\mathrm{LAI}^{\mathrm{comp}}(\Omega_i) = \lambda^{\mathrm{est}} \frac{\mathrm{PVI}\left(\vec{L}(\Omega_i)\right)}{\mathrm{PVI}\left(\vec{L}_V^{\mathrm{est}}\right)}$$

The absolute and relative errors $|\mathrm{LAI}^{\mathrm{ex}}(\Omega_i)| - \mathrm{LAI}^{\mathrm{comp}}(\Omega_i)|$ and $|\mathrm{LAI}^{\mathrm{ex}}(\Omega_i)| - \mathrm{LAI}^{\mathrm{comp}}(\Omega_i)|/\mathrm{LAI}^{\mathrm{ex}}(\Omega_i)$ as well as the mean value of these two errors for the 15 pixels Ω_i are calculated. The two later values are noted:

$$\mathrm{Error(LAI)} \quad \text{and} \quad \mathrm{Rel\ Error(LAI)} \tag{8}$$

Furthermore, we compute the mean of the rms value of the error on the input parameters:

$$\mathrm{Error(inputs)} = \left[\left(\frac{d\lambda}{\lambda}\right)^2 + \left(\frac{da}{a}\right)^2 + \left(\frac{db}{b}\right)^2 + \left(\frac{dL_V^{\mathrm{vis}}}{L_V^{\mathrm{vis}}}\right)^2 + \left(\frac{dL_V^{\mathrm{nir}}}{L_V^{\mathrm{nir}}}\right)^2\right]^{1/2} \Bigg/ \left[\lambda^2 + a^2 + b^2 + \left(L_V^{\mathrm{vis}}\right)^2 + \left(L_V^{\mathrm{nir}}\right)^2\right]^{1/2} \tag{9}$$

Figure 7 represents the 200 values of (8) with $w = 50\%$ of forest cover with the forest plots A, B and C.

We observe that Error(LAI) and Rel Error(LAI) increase with Error(inputs) with a large dispersion around a straight line. The mean ordinate of these sets of 200 points is:

– mean Error(LAI) = 0.57 (for an exact LAI equal to $\lambda_A/2 = 3$, since $w = 50\%$) corresponding to the mean of Error(input) = 8.8%, with plot A,
– mean Error(LAI) = 0.49 (for an exact LAI equal to 2.5) corresponding to the mean of Error(input) = 8.9%, with plot B,
– mean Error(LAI) = 0.32 (for an exact LAI equal to 2.7) corresponding to the mean of Error(input) = 7.8%, with plot C.

In the following, for easier notation, we shall note again Error(LAI), Rel Error(LAI) and Error(inputs), the mean of these values for the 200 random outputs.

These last values are systematically reported in table 2, for different values of w, with or without the use of the shadow function. This table shows that the absolute error on the LAI is, in the mean, very stable, almost independently of the type of forest, around 0.5, in LAI units. The relative error is just affected by the exact LAI, which depends only on w. The role of shadow is weak in the estimation of the LAI. The quality of the formula (1) is well described by this table, which shows that for a mean error of 8% on the inputs, we have an error of 0.5 on the LAI of mixed pixels. To have an idea of the behaviour of the formula with other values as 8% on the inputs, we have reproduced the previous procedure for other values of the standard deviations defined by the multiplication of (5), (6) and (7) by the same constant number. We obtain figure 8, which shows a regular decreasing of Error(LAI) with respect to Error(inputs). This figure can be useful in practice if we have a numerical estimation of Error(inputs). This estimation is guided if some inputs have a smaller influence on the result compared with others.

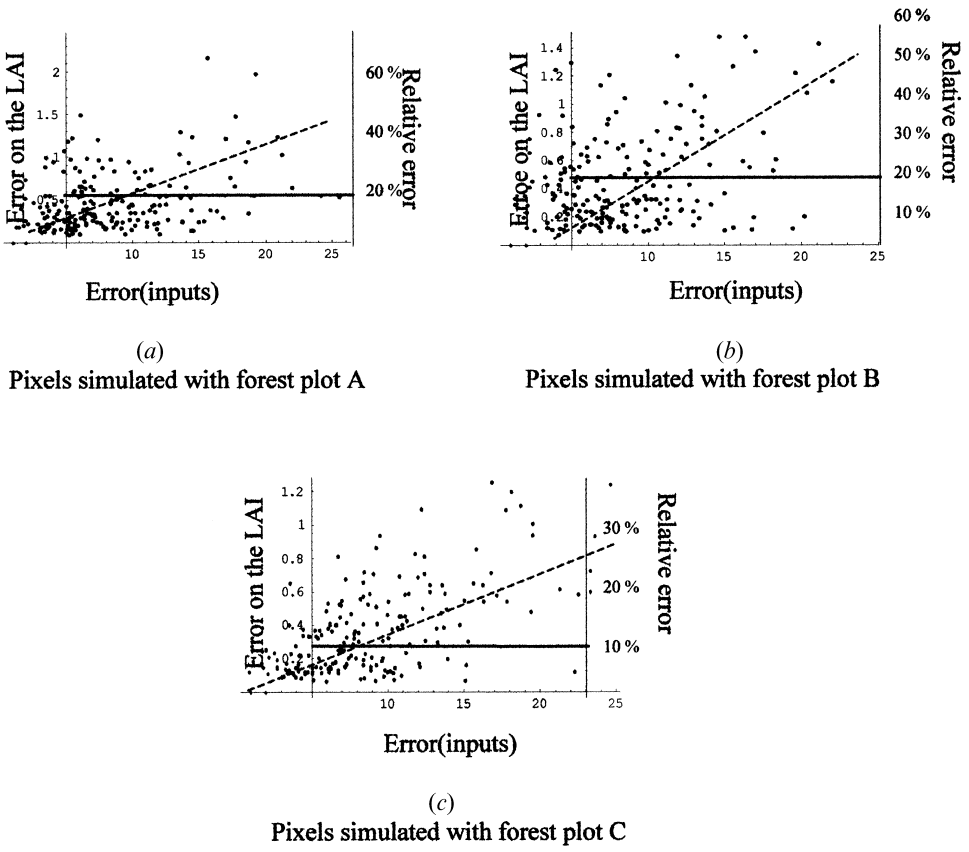

Figure 7. The errors Error(LAI) and Rel Error(LAI) (see (8)) represented for 200 outputs coming from inaccurate inputs. In abscissa, the error on the inputs computed for each outcome by Error(inputs), defined by (9). The dashed line is a weak tendency. The continuous horizontal lines express the mean values of the errors. For the three cases, $w = 50\%$. (*a*) (respectively, (*b*) and (*c*)) Pixels composed with forest plot A (respectively, B and C).

6.2. *Sensitivity of (1) with respect to each input*

To study the separate roles of the inputs on the errors, there are at least two ways. By the same technique, if we select just one parameter to be drawn at random, the others taking their optimal or exact value, we obtain the results of table 3 calculated for $w = 50\%$ and the standard deviations defined by (5), (6), (7). It shows that Error(LAI) is twice more sensitive to an error on the slope a of the soils line, or on the near-infrared measurement L_V^{nir}, than on the values of λ, b or L_V^{vis}. The fact that the role of λ is not very important is a good opportunity, since this value is the unique value to be estimated on the basis of terrain experiments.

A second, more systematic, way to study this separate dependence is to calculate the differential of (4). That leads to

$$d\left(\lambda.\frac{\text{PVI}\left(\vec{L}(\Omega)\right)}{\text{PVI}\left(\vec{L}_V\right)}\right)=\lambda\frac{\text{PVI}\left(\vec{L}(\Omega)\right)}{\text{PVI}\left(\vec{L}_V\right)}\left[\rho_\lambda\frac{d\lambda}{\lambda}+\rho_a\frac{da}{a}+\rho_b\frac{db}{b}+\rho_{L_V^{\text{vis}}}\frac{dL_V^{(\text{vis})}}{L_V^{(\text{vis})}}+\rho_{L_V^{\text{nir}}}\frac{dL_V^{(\text{nir})}}{L_V^{(\text{nir})}}\right]$$

Table 2. Quality of formula (1) giving the LAI of mixed pixels, in operational use. All the values correspond to averaged values of 200 random simulations. The last column is the relative error of the inputs in the rms sense. The relative error on the LAI is affected by the value of the LAI, directly related to w.

Simulated pixels with shadow or without		Forest cover w (%)	Relative error on the LAI: Rel Error(LAI) (%)	Absolute error on the LAI (in LAI units): Error(LAI)	Relative error on the whole inputs: Error (inputs) (%)
Forest plot A	with	20	43.3	0.5	8.7
		50	16.5	0.5	9.1
		80	13.1	0.6	8.5
	without	20	45.5	0.5	8.8
		50	17.3	0.5	8.8
		80	13.5	0.5	8.9
Forest plot B	with	20	46.9	0.5	8.9
		50	17.2	0.4	8.8
		80	13.5	0.5	8.9
	without	20	48	0.5	8.9
		50	17.9	0.4	8.8
		80	13	0.5	8.7
Forest plot C	with	20	30.4	0.3	8.5
		50	13.2	0.3	8.5
		80	11.9	0.5	8.7
	without	20	33.1	0.3	8.6
		50	14.1	0.4	8.6
		80	11.6	0.5	8.6

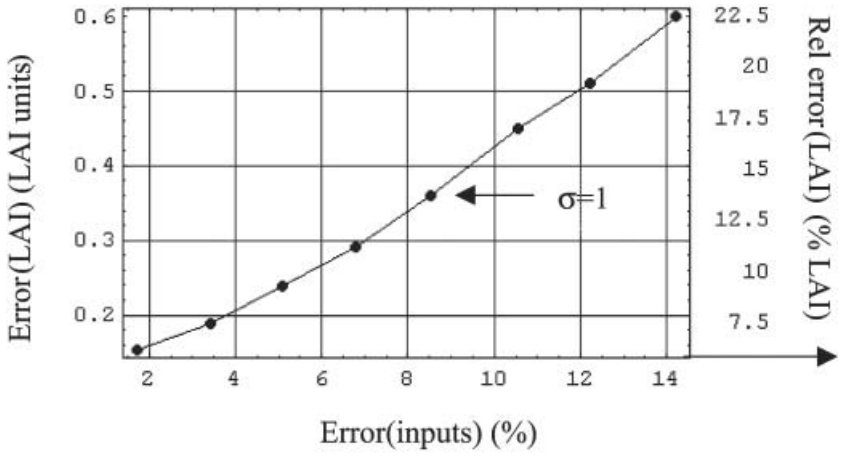

Figure 8. Error (8) on the LAI when all the inputs have an error (9) which varies following a normal law. The standard deviations are given by the values defined by (5), (6) and (7), multiplied by the same parameter σ taking successively eight values ($\sigma = 0.2$ to 1.6, by step 0.2). The point marked by an arrow corresponds to $\sigma = 1$, then to the errors reported previously (table 2) (more precisely, in the case of forest plot C, $w = 50\%$, with shadow effect).

Table 3. Separate roles of each input fluctuation on the LAI accuracy. The values are mean values, for 200 pixels drawn at random, covered by $w=50\%$ forest. The mean fluctuations on the inputs, considered separately, are: mean$(d\lambda/\lambda)=2.1$; mean$(da/a)=0.2$; mean$(db/b)=0.2$; mean$\left(d\,L_V^{\mathrm{vis}}/L_V^{\mathrm{vis}}\right)=0.1$; mean$\left(d\,L_V^{\mathrm{nir}}/L_V^{\mathrm{nir}}\right)=0.1$.

Forest plot A Error due to fluctuations of:	λ	a	b	L_V^{vis}	L_V^{nir}
Error(LAI)	0.18	0.37	0.19	0.17	0.39
RelError(LAI) (%)	5.8	12.2	6.3	5.6	12.9
Forest plot B Error due to fluctuations of:					
Error(LAI)	0.13	0.34	0.15	0.12	0.32
RelError(LAI) (%)	5.3	13.7	5.9	4.9	13.1
Forest plot C Error due to fluctuations of:					
Error(LAI)	0.14	0.22	0.13	0.11	0.31
RelError(LAI) (%)	5.5	8.6	4.8	4.5	11.7

where the amplification factors ρ are:

$$\rho_\lambda = 1$$

$$\rho_a = \frac{a}{\sqrt{a^2+1}}\left[\frac{L_V^{(\mathrm{vis})}}{\mathrm{PVI}\left(\vec{L}_V(\Omega)\right)} - \frac{L^{(\mathrm{vis})}}{\mathrm{PVI}\left(\vec{L}(\Omega)\right)}\right]$$

$$\rho_b = \frac{b}{\sqrt{a^2+1}}\left[\frac{1}{\mathrm{PVI}\left(\vec{L}_V(\Omega)\right)} - \frac{1}{\mathrm{PVI}\left(\vec{L}(\Omega)\right)}\right]$$

$$\rho_{L_V^{\mathrm{vis}}} = \frac{L_V^{(\mathrm{vis})}}{\sqrt{a^2+1}}\left[\frac{a}{\mathrm{PVI}\left(\vec{L}_V(\Omega)\right)}\right]$$

$$\rho_{L_V^{\mathrm{nir}}} = \frac{L_V^{(\mathrm{nir})}}{\sqrt{a^2+1}}\left[\frac{-1}{\mathrm{PVI}\left(\vec{L}_V(\Omega)\right)}\right]$$

The numerical values of the amplification factors are calculated with the data of the three forest plots A, B and C with the shadow effect. They are given in table 4. This table explains the previous results. For $w=50\%$ of vegetation we find the results obtained by simulation (table 3). We remark that in table 3, the sum of the values Error(LAI) for all the inputs is significantly larger than the values observed when all the parameters vary (table 2). The signs of the amplification factors

Table 4. Amplification factors. These values confirm the sensitivity of the formula to the input parameters a (slope of the soils line) and L_V^{nir} (the near-infrared estimation of the forest radiometry), as was observed after the simulations (table 3).

	ρ_λ	ρ_a	ρ_b	$\rho_{L_V^{\mathrm{vis}}}$	$\rho_{L_V^{\mathrm{nir}}}$
$w=20\%$	1	−2.69	−0.71	0.16	−1.34
$w=50\%$	1	−0.65	−0.17	0.16	−1.34
$w=80\%$	1	−0.16	−0.04	0.16	−1.34

(table 4) show the reason. Indeed, when the fluctuations on the data play all together, some play by increasing the error on the LAI, others have the opposite effect. We suspected this type of situation (§5.4) with the shadow, angular and atmospheric combined effects. The confirmation of the importance of the accurate determination of the value L_V^{nir} is given, for any cover percentage of the pixel. A good estimation of the parameter a is more useful for a weak than for an important cover. These observations hold for the three forest plots and without shadow effect, at a few percentage differences. The error on the experimental estimation of λ is not amplified by the formula, since $\rho_\lambda = 1$.

Finally, the simulation of the operational use of the formula (1) to compute the LAI of mixed pixels shows a good accuracy, even with rough approximations of the inputs. The shadow effect, which is not easy to estimate in practice has a weak effect on the result, mainly affected by the near-infrared estimation of the vegetation radiometry and the slope of the soils line. It appears that the asymptotic estimation λ of the homogeneous forest LAI is not the main source of error in the LAI of mixed regions.

7. Conclusions

We proved, on the basis of terrain, airborne and satellite measurements, the validity and the quite good accuracy of a formula for the computation of the LAI of mixed pixels. The formula uses the classical visible and near-infrared radiometric channels and is adapted to regions covered with forest and bare soils. This composition can be extended to other types of homogeneous vegetation and bare soils, provided we have an estimation of the LAI of this type of vegetation.

The scale and spatial resolution, which come into play in the observation of Earth by remote sensing, make almost impossible any complete validation of the models. The heterogeneity of the surface parameters is the main cause of this difficulty. First, the definition of the input parameters is itself a problem, not always solved. For example the surface temperature of a heterogeneous surface does not have, up to now, a satisfactory definition; or the definition of the soils line depends, not only on the soils, but also on the sensor's resolution. Secondly, the validation needs a comparison between the outputs of the model and the *in situ* measurements of these output parameters. This is generally impossible, taking into account the difference of the involved scales.

In the model studied in this paper, these two difficulties had been naturally encountered. The inputs are both radiometric and obtained by terrain samples of the LAI. Their definition is attached to the soils line, the knowledge of the forest radiometry and to what means a homogeneous forest with respect to the LAI. After a confirmation of the perfect accuracy of the formula in ideal homogeneous cases, we introduced these uncertainties, using a Gaussian simulation.

The second difficulty, which concerns the main aspect of the model validation, is the comparison between the LAI as the output of the model and the exact *in situ* one. To obtain this last value, we used terrain experiments. The radiometry used airborne and satellite data. We simulated the ground surface in terms of LAI and radiometry, at high resolution. We have considered the role of the sparseness of the forest with its consequence on the shadow, the error on the knowledge of the soils line, on the vegetation radiometry and the radiometric heterogeneity of the homogeneous forest in terms of LAI.

The numerical results show that the LAI of mixed regions constituted of homogeneous forest with respect to the LAI and various bare soils, can be

computed in a robust way. The various errors involved in the input data are not amplified by the formula. The given quantitative errors estimations cannot be used numerically, as they are, but can nevertheless give a good idea of the accuracy of the LAI computations.

Acknowledgments

We want to thank the two anonymous referees for their fruitful comments. This paper was supported by the National Program of Remote Sensing of the CNRS (Contract number 98 RR1/0169).

References

CRACKNELL, A. P., and HAYES, L. W. B., 1993, *Introduction to Remote Sensing* (London: Taylor and Francis).

DUFRÊNE, E., and BRÉDA, N., 1995, Estimation of deciduous forest leaf area index using direct and indirect methods. *Oecologia*, **104**, 156–162.

HAPKE, B., 1993, *Theory of Reflectance and Emittance Spectroscopy* (Cambridge: Cambridge University Press).

KAUFMAN, Y. J., 1989, *Theory and Applications of Optical Remote Sensing*, edited by G. Asrar (New York: John Wiley & Sons).

LEBLANC, G. S., CHEN, J. M., WHITE, H. P., CHILAR, J., LACAZE, R., ROUJEAN, J.-L., and LATIFOVIC, R., 2001, Mapping vegetation clumping index from directional satellite measurements. *8th International Symposium on Physical Measurements and Signatures in Remote Sensing, 8–12 January 2001, Aussois, France*, pp. 450–459.

NIZINSKY, J. J., and SAUGIER, B., 1988, A model of leaf budding and development for a mature Quercus forest. *Journal of Applied Ecology*, **25**, 643–655.

RAFFY, M., SOUDANI, K., and TRAUTMANN, J., 2003, On the variability of the LAI of homogeneous covers with respect to the surface size and application. *International Journal of Remote Sensing*, **24**, 2017–2035.

RICHARDSON, A. J., and WIEGAND, C. L., 1977, Distinguishing vegetation from soil background information. *Photogrammetric Engineering and Remote Sensing*, **43**, 1541–1552.

SABATIER, C., 1989, Production de taillis châtaignier (Castanea sativa, Mill) en relation avec les caractéristiques stationnelles. Thèse de doctorat, Université de Paris-Sud, France.

SCHOWENGERDT, R. A., 1997, *Remote Sensing* (San Diego, CA: Academic Press).

WARREN WILSON, J., 1959, Analysis of spatial distribution of foliage by two-dimensional point quadrats. *New Phytologist*, **58**, 92–101.

WARREN WILSON, J., 1960, Inclined point quadrats. *New Phytologist*, **59**, 1–8.

WARREN WILSON, J., 1963, Estimation of foliage denseness and foliage angle by inclined point quadrat. *Australian Journal of Botany*, **11**, 95–105.